A Study of Turbulent Flow Downstream of an Abrupt Pipe Expansion

R. S. Amano*
The University of Wisconsin, Milwaukee, Wisconsin

A numerical study is reported of heat transfer in the separated flow region created by an abrupt pipe expansion. Computations have employed a hybrid method of central and upwind finite differencing to solve the full Navier-Stokes equations with the $k-\epsilon$ turbulence model. The study has given its main attention to the simulation of the region in the immediate vicinity of the wall, by formulating a near-wall model for the evaluation of the mean generation and destruction rate of the ϵ equation. The computed results were compared with the experimental data. The results showed generally encouraging agreement with the measurements.

Nomenclature

C_μ, C_1, C_2, C_ℓ = coefficients in turbulence model
c_p = specific heat at constant pressure
D = diameter of pipe downstream of expansion
d = diameter of pipe upstream of expansion
E = empirical constant in logarithmic law
H = step height, $=(D-d)/2$
k = turbulent kinetic energy, $=\overline{u_i^2}/2$
Nu = Nusselt number based on diameter of pipe downstream of expansion
P = turbulence energy generation rate
$\mathcal{P}$ = P function
p = pressure
$\dot{q}_w''$ = wall heat flux
Re_D = Reynolds number based on diameter of pipe downstream of expansion
Rv = viscous sublayer Reynolds number, $=20.0$
r = radial coordinate
St = Stanton number
T = temperature
U = mean velocity in x direction
u = turbulent fluctuating velocity
V = mean velocity in r direction
x = coordinate parallel to pipe axis
y = distance from pipe wall
y^+ = dimensionless distance, $=yk^{1/2}/\nu$
Γ_{eff} = effective diffusivity
ϵ = dissipation rate of turbulence energy, $=\nu\overline{(\partial u_i/\partial x_j)^2}$
κ = von Kármán constant
μ = dynamic viscosity
μ_{eff} = effective viscosity, $=\mu+\mu_t$
μ_t = turbulent dynamic viscosity
ν = kinematic viscosity
ν_t = turbulent kinematic viscosity
ρ = density
σ = Prandtl number
$\sigma_k, \sigma_\epsilon, \sigma_T$ = turbulent Prandtl numbers for diffusion of k, ϵ, and temperature
τ_t = turbulent shear stress
ϕ = dependent variables (U, V, k, and ϵ)

Subscripts

i,j = tensor notation
k,ϵ = values pertaining to kinetic energy and dissipation rate, respectively
N = values at node point N
n = values at the edge of wall adjacent cell
P = values at node point P
t = turbulent values of quantity
v = values at the edge of viscous sublayer
w = wall values

Presented as Paper 82-1269 at the AIAA/SAE/ASME 18th Joint Propulsion Conference, Cleveland, Ohio, June 21-23, 1982; submitted July 1, 1982; revision submitted Jan. 6, 1983.

*Professor, Mechanical Engineering Department.

Introduction

HEAT and mass transfer in pipe flows normally take place as a thin shear or boundary-layer type flow which can be analyzed in terms of parabolic equation systems. On the other hand, if there are any sudden expansions or obstructions in the pipe flow, local separation will take place and the flow immediately following the obstruction will be recirculating. Locally this will then require a formulation of an elliptic equation system. The latter system is also seen in the combustion processes of gas turbine, ramjets, and many types of industrial furnaces. In these cases, the flow is recirculating in some parts of the domain, turbulent, steady, and two dimensional.

Several experimental studies[1-3] have shown that for an abrupt expansion in diameter of flow passage in pipes or in the combustion chamber, on the downsteam side, the levels of heat/mass-transfer coefficient are several times greater than that for fully-developed turbulent flow at the same Reynolds number. The reason for this heat/mass-transfer augmentation may be attributed to an increase in the levels of the turbulence energy.

In this paper the study has given its main attention to the simulation of the region in the immediate vicinity of the wall. The near-wall model developed here is based on the model of Chieng and Launder[4] except that the local variation of turbulence quantities are evaluated in the ϵ equation in this paper. The inflow/outflow and boundary conditions are well defined. The results were compared with the measured data of Zemanick and Dougall.[1] The model in this paper improved predictions of heat-transfer coefficients approximately 20% on the model of Chieng and Launder.

Mathematical and Physical Models

Governing Equations

The present work is based on the numerical solutions of the two-dimensional form of the time-averaged Navier-Stokes equations. Turbulent viscosity is defined by the high Reynolds number version of the $k-\epsilon$ model of turbulence (see Table 1).

Table 1 Summary of equations solved

Equation	ϕ	Γ_{eff}	S_ϕ
Continuity	1	0	0
x momentum	U	μ_{eff}	$-\frac{\partial p}{\partial x}+\frac{\partial}{\partial x}\left(\mu_{\text{eff}}\frac{\partial U}{\partial x}\right)+\frac{1}{r}\frac{\partial}{\partial r}\left(r\mu_{\text{eff}}\frac{\partial V}{\partial x}\right)$
r momentum	V	μ_{eff}	$-\frac{\partial p}{\partial r}+\frac{\partial}{\partial x}\left(\mu_{\text{eff}}\frac{\partial U}{\partial r}\right)+\frac{1}{r}\frac{\partial}{\partial r}\left(r\mu_{\text{eff}}\frac{\partial V}{\partial r}\right)-2\mu_{\text{eff}}V/r^2$
Thermal energy	T	$\frac{\mu}{\sigma}+\frac{\mu_t}{\sigma_T}$	0
Turbulence energy	k	$\mu+\frac{\mu_t}{\sigma_k}$	$\rho P-\rho\epsilon$
Energy dissipation	ϵ	$\mu+\frac{\mu_t}{\sigma_\epsilon}$	$C_1\frac{\rho\epsilon}{k}P-C_2\frac{\rho\epsilon^2}{k}$

where

$$\mu_t = C_\mu \rho k^2/\epsilon$$

and

$$P=\nu_t\left[\left(\frac{\partial U}{\partial r}+\frac{\partial V}{\partial x}\right)^2+2\left(\frac{\partial U}{\partial x}\right)^2+2\left(\frac{\partial V}{\partial r}\right)^2+2\left(\frac{V}{r}\right)^2\right]$$

and where

C_μ	C_1	C_2	σ_k	σ_ϵ
0.09	1.44	1.92	1.0	1.3

The governing equation following this approach for the present flow configuration can be written in the following general form:

$$\frac{1}{r}\left[\frac{\partial}{\partial x}(r\rho U\phi)+\frac{\partial}{\partial r}(r\rho V\phi)\right] = \frac{1}{r}\left[\frac{\partial}{\partial x}\left(r\Gamma_{\text{eff}}\frac{\partial\phi}{\partial x}\right)+\frac{\partial}{\partial r}\left(r\Gamma_{\text{eff}}\frac{\partial\phi}{\partial r}\right)\right]+S_\phi \quad (1)$$

All of the governing equations used in the present paper and the constants used in the turbulence model are given in Table 1. With the high Reynolds number formulation, levels of near-wall kinetic energies and dissipation rates are obtained as described in the following subsection.

Near-Wall Model for High Reynolds Numbers

While viscous effects on the energy-containing turbulence motions are negligible throughout most of the flow, the no-slip condition at a solid interface always ensures that, in the immediate vicinity of a wall, viscous effects will be influential. Although the thickness of this viscous-affected zone is usually two or more orders of magnitude smaller than the overall width of the flow, its effects extend over the whole flowfield since, typically, 50% of the velocity change from the wall to the freestream occurs in this region.

The near-wall model which evaluates the mean generation rate and mean dissipation rate in the k equation in the numerical cell adjacent to the wall was proposed by Chieng and Launder.[4] This model was applied to the computation of a turbulent impinging jet by Amano and Neusen.[5] In this model, as can be seen in Fig. 1, a parabolic variation of the turbulent kinetic energy is assumed which corresponds to a linear increase of fluctuating velocity with distance from the wall within the viscous sublayer. Then the turbulent kinetic energy k varies linearly towards the outer node points. Unlike

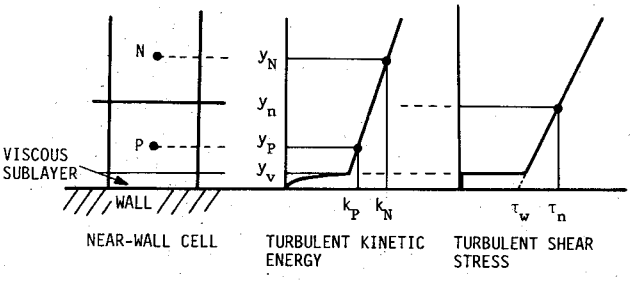

Fig. 1 Near-wall physical model.

the turbulent kinetic energy the turbulent shear stress τ_t is zero within the viscous sublayer and τ_t undergoes an abrupt increase at the edge of the sublayer while varying linearly over the remainder of the cell. The details of this treatment of the k equation are given in Ref. 4. However, these variations of the turbulence quantities are considered only in the k equation but not in the ϵ equation. In the ϵ equation the value of ϵ in the wall-adjacent cell was approximated under local equilibrium condition as

$$\epsilon = k_p^{3/2}/C_\ell y \quad (2)$$

instead of evaluating its value by taking the local variations of k, ϵ, and τ_t into account.

In the present study, the treatment of the k equation in the near-wall cell described above is developed further for the ϵ equation by using the wall function treatment since the behavior of ϵ is significant considering that ϵ near the wall is an order of magnitude larger than that in the fully-turbulent core and reaches its maximum at the wall. Each term in the ϵ equation should be evaluated in accordance with the k equation, rather than being approximated under local equilibrium conditions. The procedure of a development of this model is described subsequently.

In the viscous sublayer and in the fully-turbulent region, turbulence energy k and energy dissipation rate ϵ are expressed with the notation in Fig. 1 as follows:

Viscous sublayer

$$k=k_v\left(\frac{y}{y_v}\right)^2 \qquad \epsilon=2\nu\left(\frac{\partial k^{1/2}}{\partial y}\right)^2 \tag{3}$$

Fully-turbulent region

$$k=\frac{k_n-k_v}{y_n-y_v}y+\left(k_P-\frac{k_P-k_N}{y_P-y_N}y_P\right)=by+a \qquad \epsilon=k^{3/2}/C_\ell y \tag{4}$$

The terms in the ϵ equation [see Eq. (1) and Table 1] represent an ϵ balance involving convective transport, diffusion, generation, and destruction of energy dissipation. The convective terms, which will generally be of minor influence near the wall, are handled in such a way that all fluid leaving the cell is assumed to have the energy at node P. Likewise, the diffusion terms can be treated similarly. Noting the expression of Eq. (3) for ϵ inside a viscous sublayer, ϵ has zero gradient at the wall as does k since ϵ is constant in the viscous sublayer. This fact corresponds to no diffusion of energy dissipation to the wall. The diffusional flux of energy dissipation out of the cell at its north, west and east boundaries (Fig. 1) are handled by the same differencing scheme that is employed over the remainder of the flow.

The mean generation and destruction rates in the ϵ equation can be obtained as follows: over the fully-turbulent region, the main velocity parallel to the wall is assumed to vary with distance from the wall according to

$$\frac{Uk_v^{1/2}}{\tau_w/\rho}=\frac{1}{\kappa^*}\log(E^*yk_v^{1/2}/\nu) \tag{5}$$

where $\kappa^*=\kappa C_\mu^{1/4}$ and $E^*=EC_\mu^{1/4}$. The generation rate of the k equation can be written as

$$P\equiv\tau_t\left(\frac{\partial U_i}{\partial x_j}+\frac{\partial U_j}{\partial x_i}\right) \tag{6}$$

Since the turbulent shear stress is zero within the viscous sublayer, the mean generation rate of ϵ can be expressed as

$$\overline{\left(C_1\frac{\epsilon}{k}P\right)}=\frac{1}{y_n}\int_{y_v}^{y_n}C_1\frac{(by+a)^{1/2}}{C_\ell y}\left[\tau_w+(\tau_n-\tau_w)\frac{y}{y_n}\right]\times\left(\frac{\partial U}{\partial y}+\frac{\partial V}{\partial x}\right)\mathrm{d}y \tag{7}$$

where Eqs. (4) and (6) are used.

By using Eq. (5) for the main velocity distribution, we can obtain

$$\begin{aligned}\overline{\left(C_1\frac{\epsilon}{k}P\right)}=&\frac{\tau_w}{\rho}\frac{C_1}{k_v^{1/2}\kappa^*C_\ell y_n}\left[\tau_w\left(\frac{k_v^{1/2}}{y_v}-\frac{k_n^{1/2}}{y_n}+\frac{b}{2}\lambda\right)\right.\\&\left.+\frac{\tau_n-\tau_w}{y_n}\{2(k_n^{1/2}-k_v^{1/2})+a\lambda\}\right]\\&+\frac{C_1}{C_\ell y_n}\left[\tau_w\{2(k_n^{1/2}-k_v^{1/2})+a\lambda\}\right.\\&\left.+\frac{2}{3}\frac{\tau_n-\tau_w}{y_n}\frac{1}{b}(k_n^{3/2}-k_v^{3/2})\right]\frac{\partial V}{\partial x}\end{aligned} \tag{8}$$

where

$$\lambda=\frac{1}{(a)^{1/2}}\log\left[\frac{(k_n^{1/2}-a^{1/2})(k_v^{1/2}+a^{1/2})}{(k_v^{1/2}-a^{1/2})(k_n^{1/2}+a^{1/2})}\right] \qquad (a>0)$$

$$=\frac{1}{(-a)^{1/2}}\left[\tan^{-1}\left(\frac{k_n}{-a}\right)^{1/2}-\tan^{-1}\left(\frac{k_v}{-a}\right)^{1/2}\right] \qquad (a<0) \tag{9}$$

Unlike the generation rate of the ϵ equation, the destruction rate of the ϵ equation is not zero in the viscous sublayer. In the viscous sublayer, by using Eq. (3), the average of k can be obtained as

$$\frac{1}{y_v}\int_0^{y_v}k\mathrm{d}y=\frac{k_v}{3} \tag{10}$$

and the mean destruction rate is expressed as

$$\overline{\left(C_2\frac{\epsilon^2}{k}\right)}=\frac{12C_2\nu^2k_v}{y_v^3y_n} \tag{11}$$

To evaluate the destruction rate in the fully-turbulent region, we integrate $(C_2\epsilon^2/k)$ between y_v and y_n. After including the linear variation of k in Eq. (4) and the contribution of destruction in the viscous sublayer given in Eq. (11), the mean rate is given as

$$\overline{\left(C_2\frac{\epsilon^2}{k}\right)}=\frac{12C_2}{y_ny_v}\left(\frac{k_v}{Rv}\right)^2+\frac{(1-y_v/y_n)C_2}{C_\ell^2}\times\left(\frac{a^2}{y_vy_n}+\frac{2ab}{y_n-y_v}\log\frac{y_n}{y_v}+b^2\right) \tag{12}$$

where a and b are given in Eq. (4), and where

$$Rv\equiv\frac{y_vk_v^{1/2}}{\nu} \tag{13}$$

The near-wall model developed here is summarized in Table 2.

The interlinkage used between the near-wall variation and the local wall fluxes for heat is given as

$$\frac{\rho c_p(T-T_w)k_v^{1/2}}{\dot{q}_w''}=\left(\frac{U_vk_v^{1/2}}{\tau_w/\rho}+\mathcal{P}\right) \qquad \text{heat flux} \tag{14}$$

where $\mathcal{P}$ is the P function given by Jayatilleke[6] as

$$\mathcal{P}=5.0[(\sigma/\sigma_T)^{0.75}-1][1+0.28\exp(-0.007\sigma/\sigma_T)] \tag{15}$$

where σ_T is the turbulent Prandtl number equal to 0.9.

Numerical Solution Procedure

The method adopted for solving Eq. (1) is the solution procedure of the TEACH code. In this program the value of each scalar quantity is associated with every grid node (i.e., the points where the grid lines intersect), although the vector quantities (velocity components) are displaced in space relative to the scalar quantities p, T, k, and ϵ. Such a staggered grid system is advantageous in solving the velocity field since the pressure gradients are easy to evaluate and velocities are conveniently located for the calculation of convective fluxes. According to Gosman et al.,[7] a hybrid scheme is adopted in which a central difference approximation is used when the intercell Peclet number is less than 2 and an upwind difference of the combined effect of convection and diffusion is employed at the stronger level of

Table 2 Near-wall model

Generation rate in k equation, $\bar{P}$

$$\frac{\tau_w(U_n-U_v)}{y_n}+\frac{\tau_w(\tau_n-\tau_w)}{\rho\kappa^* k_v^{1/2} y_n}\left(1-\frac{y_v}{y_n}\right)+\left[\tau_w\left(1-\frac{y_v}{y_n}\right)+\frac{\tau_n-\tau_w}{2}\left(1-\left(\frac{y_v}{y_n}\right)^2\right)\right]\frac{\partial V}{\partial x}$$

Dissipation rate in k equation, $\bar{\epsilon}$

$$\frac{2k_v^{3/2}}{y_n Rv}+\frac{1}{y_n C_\ell}\left[(2/3)(k_n^{3/2}-k_v^{3/2})+2a(k_n^{1/2}-k_v^{1/2})+a^2\lambda\right]$$

Generation rate in ϵ equation, $\overline{(C_1 P\epsilon/k)}$

$$\frac{\tau_w}{\rho}\frac{C_1}{k_v^{1/2}\kappa^* C_\ell y_n}\left[\tau_w\left(\frac{k_v^{1/2}}{y_v}-\frac{k_n^{1/2}}{y_n}+\frac{b}{2}\lambda\right)+\frac{\tau_n-\tau_w}{y_n}(2(k_n^{1/2}-k_v^{1/2})+a\lambda)\right]$$

$$+\frac{C_1}{C_\ell y_n}\left[\tau_w(2(k_n^{1/2}-k_v^{1/2})+a\lambda)+\frac{2}{3}\frac{\tau_n-\tau_w}{y_n}\frac{1}{b}(k_n^{3/2}-k_v^{3/2})\right]\frac{\partial V}{\partial x}$$

Destruction rate in ϵ equation, $\overline{(C_2\epsilon^2/k)}$

$$C_2\left[\frac{12}{y_n y_v}\left(\frac{k_v}{Rv}\right)^2+\frac{1-y_v/y_n}{C_\ell^2}\left(\frac{a^2}{y_v y_n}+\frac{2ab}{y_n-y_v}\log\frac{y_n}{y_v}+b^2\right)\right]$$

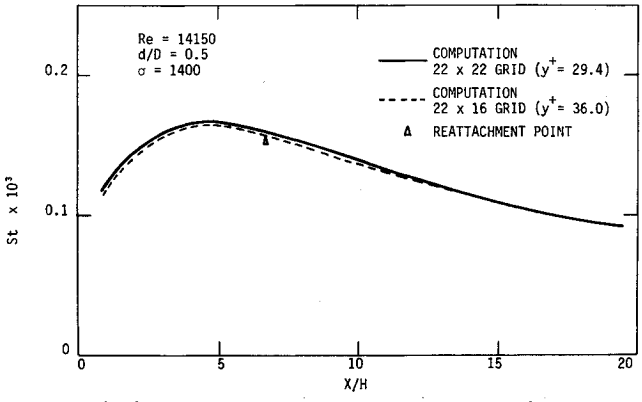

Fig. 2 Stanton number distribution along the pipe.

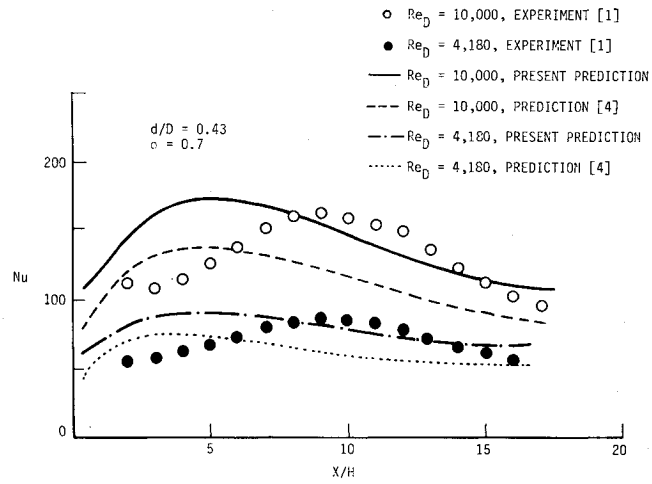

Fig. 3 Nusselt number distribution along the pipe for $d/D=0.43$.

convection (Peclet number is greater than 2). Two problems of determining the pressure distribution and satisfying continuity are overcome by adjusting the pressure field so as to satisfy continuity. This is the so-called semi-implicit method for pressure linked equations (SIMPLE) algorithm developed by Patankar and Spalding.[8]

The majority of the computations were performed with a 22×16 variable grid system which provides finer grid near the wall. Central processor times on a UNIVAC 1100 computer were about 3 min to converge, which was achieved typically after 140 iterations. One computation was made with a 22×22 grid. Differences in predicted Stanton number between these two node densities did not exceed 1% as is shown in Fig. 2. The values of y^+ specified in Fig. 2 are the smallest values of all the near-wall nodal points. The fact assures that the model developed here is almost independent of the grid system.

Results and Discussion

The near-wall model developed in the preceding section is adopted for the computation of heat-transfer rate along the pipe downstream from an abrupt pipe expansion. For any particular computing run, as shown in Fig. 2, the heat-transfer coefficients start at a low level, increase as one moves away from the expansion, reach a peak 5-6 step heights from the expansion and then decrease, eventually reaching the fully-developed condition. As is depicted in Fig. 2, the maximum Stanton number in fact does not coincide with the reattachment point but occurs about 1-1.5 step heights upstream therefrom.

The computed results of heat-transfer rate of low Prandtl number ($\sigma=0.7$) are compared with the experimental data obtained by Zemanick and Dougall[1] over a wide range of Reynolds number ($Re=4{,}180$-$48{,}000$) for two different expansion ratios. Figure 3 compares the computed results with the experimental data for $d/D=0.43$ and Fig. 4 compares those for $d/D=0.54$, respectively. In these two figures the computed results of Chieng and Launder[4] are also compared with the present model. As described in the preceding section, the difference between the present model and that of Chieng and Launder is that the local variations of turbulent quantities are taken into account for the evaluation of the ϵ equation in the present model.

For the case of smaller expansion ratio ($d/D=0.43$), as shown in Fig. 3, the computed results show the occurrence of the maximum Nusselt number approximately four step heights upstream from that of the experimental data for two

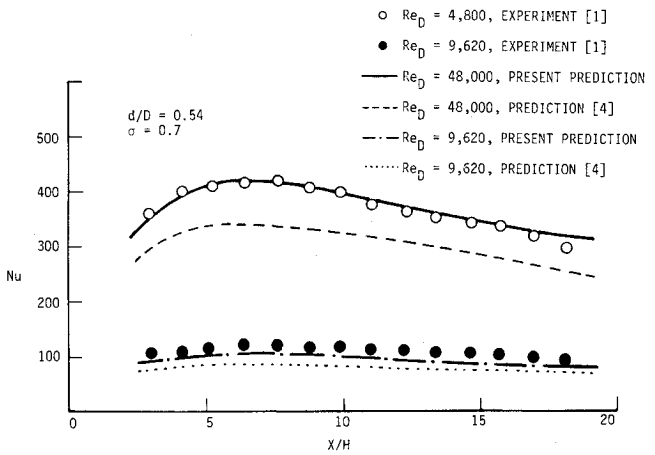

Fig. 4 Nusselt number distribution along the pipe for $d/D=0.54$.

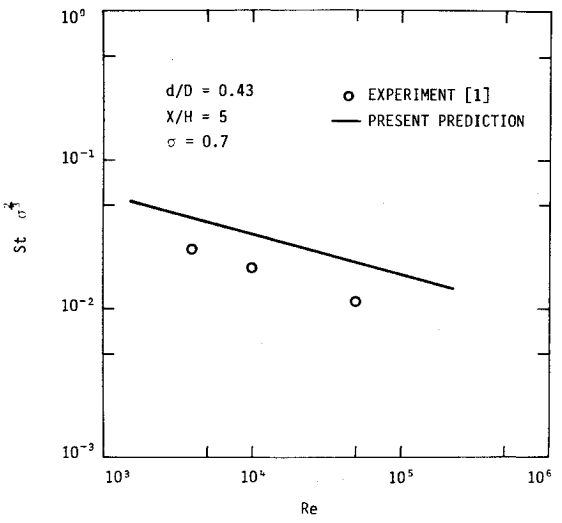

Fig. 5 Variation of Stanton number with Reynolds number.

different Reynolds numbers of 4,180 and 10,000. While the near-wall model of Ref. 4 shows the occurrence of the maximum Nusselt number approximately 5.5 step heights upstream from the measured value for $Re=4{,}180$. Although the present model does not agree with the experimental data in the prediction of the occurrence of the maximum Nusselt number, this model gives better agreement for $Re=4{,}180$ than that of Ref. 4 (i.e., the position of the maximum Nusselt number by the present model is closer to the measured value for the smaller Reynolds number flows). Another predominant distinction between these two models is the prediction in level of heat-transfer rate; the results obtained by the present model display excellent agreement with experimental data with regard to the heat-transfer level. The results obtained by the model of Ref. 4 show about 18-20% lower values than the present prediction.

Unlike the case of the expansion ratio, $d/D=0.43$, the results for $d/D=0.54$ display surprisingly better agreement with the experimental data, as shown in Fig. 4. In both near-wall models, the occurrence of the maximum Nusselt number coincides with the experimental data for Reynolds numbers of 9,620 and 48,000. Furthermore, the levels of heat-transfer rate agree well with the experimental data, especially for $Re=48{,}000$. However, the difference between the predicted and the measured values is larger (-20%) for $Re=9{,}620$. It is also noticed that the model of Ref. 4 always gives values approximately 20% lower than the present model. The reason for this difference in the prediction of heat-transfer rates in these two models may be explained by focusing on the behavior of ϵ near the wall. According to the present formulation of k, ϵ, and τ_t near the wall, the dissipation rate shows a high value within the viscous affected region and then decreases as one moves away from the wall. Consequently the average value of the energy dissipation in the wall proximity cell would be higher than that approximated by Eq. (2). This higher energy-dissipation rate tends to enhance the energy-transfer rate towards the wall.

In the foregoing discussion it has been pointed out that the agreement of the occurrence of the maximum Nusselt number between computed and measured values is excellent for $d/D=0.54$, while the discrepancy has been detected to be rather high for $d/D=0.43$. Considering that the smaller the expansion ratio the larger is the step height, the error occurred in the prediction of the spreading rate at the separated region would be amplified for the larger step height (i.e., for the smaller expansion ratio $d/D=0.43$). Thus the discrepancy due to the choice of a turbulence model would be significantly affected for $d/D=0.43$. It is worth noticing that the occurrence of the maximum Nusselt number is almost independent of Reynolds number.

With regard to the contribution of the near-wall model, although the present near-wall model has shown improvement in the prediction of the heat-transfer level, it can be said that none of the various aspects of the near-wall model developed in this study has any significant effect on the location of the peak Nusselt number. Since this location is controlled by the model in the fully-turbulent core, the prediction of this aspect can be changed by adopting a different turbulence model.

For the purpose of examining the dependency of heat-transfer rates on the flow Reynolds number, the level of Stanton number at the downstream position of $X/H=5$ for $d/D=0.43$ is plotted as a function of Reynolds number in Fig. 5. The variation of the Stanton number shown in Fig. 5 suggests that the calculated behavior exhibits slightly smaller sensitivity to Reynolds number than the measured values. Several reasons may be considered for this discrepancy between the measured and computed results. First of all it could be considered that this may arise either from the experimental setup or the numerical model, but they alone may not be responsible for the discrepancy in slope as shown in the figure. The second reason is that the discrepancy may come from the analogy between momentum and heat flux correlation [Eq. (14)]. A question arises whether the momentum heat flux correlation given by Jayatilleke is universal or not. In order to clarify the present situation let us focus on the near-wall region. For a high Reynolds number flow the length scale obtained near the reattachment zone would be relatively larger than it should be if we employ the high Reynolds number form of the $k\sim\epsilon$ model. Consequently, the larger length scales produce higher turbulent viscosities by reducing ϵ and thus increasing k and a too thin viscous sublayer, since the turbulent kinetic energy at the edge of viscous sublayer k_v will be too large. These effects combine to produce a lower thermal resistance in the near-wall layer than is actually observed, which results in higher Stanton numbers near the reattachment zone for high Reynolds number flow.

Conclusions

The main conclusions from the numerical study of the flows downstream of an abrupt expansion in a pipe are summarized as follows:

1) The near-wall model which provides physically better approximation for the evaluation of both k and ϵ equations is developed.

2) The prediction in the level of Nusselt number is improved by approximately 20% by employing the present near-wall model. However, little change has been observed in the location of the maximum Nusselt number.

3) Generally the agreement in the location of the maximum Nusselt number between the present computational model and

the experimental data is better for the diameter ratio of 0.54 than for 0.43.

4) Calculated results show that the dependency of the level of heat-transfer rate on Reynolds number is slightly smaller than the experimental data.

Acknowledgments

This work was conducted at the University of Wisconsin-Milwaukee, through the sponsorship of the NASA Ames Research Center, Moffett Field, Calif., under Contract NAG 2-160. Thanks are due to Ms. J. Amano who handled the production of the manuscript.

References

[1]Zemanick, P. P. and Dougall, R. S., "Local Heat Transfer Downstream of Abrupt Circular Channel Expansion," *ASME Journal of Heat Transfer*, Vol. 92, Feb. 1970, pp. 53-60.

[2]Krall, K. M. and Sparrow, E. M., "Turbulent Heat Transfer in the Separated Reattached and Redevelopment Regions of a Circular Tube," *ASME Journal of Heat Transfer*, Vol. 83C, 1961, p. 131.

[3]Runchal, A. K., "Mass Transfer Investigations in Turbulent Flow Downstream of Sudden Enlargement of a Circular Pipe for Very High Schmidt Numbers," *International Journal of Heat and Mass Transfer*, Vol. 14, 1971, pp. 781-792.

[4]Chieng, C. C. and Launder, B. E., "On the Calculation of Turbulent Heat Transport Downstream From an Abrupt Pipe Expansion," *Numerical Heat Transfer*, Vol. 3, 1980, pp. 189-207.

[5]Amano, R. S. and Neusen, K. F., "A Numerical and Experimental Investigation of High-Velocity Jets Impinging on a Flat Plate," *Proceedings of the 6th International Symposium on Jet Cutting Technology*, Cranfield, BHRA Fluid Engineering, April 1982, pp. 107-122.

[6]Jayatilleke, C. L., "The Influence of Prandtl Number and Surface Roughness on the Resistance of the Laminar Sub-Layer to Momentum and Heat Transfer," *Progress in Heat and Mass Transfer*, Vol. 1, 1969, pp. 193-329.

[7]Gosman, A. D., Pun, W. M., Runchal, A. K., Spalding, D. B., and Wolfshtein, M., *Heat and Mass Transfer in Recirculating Flows*, Academic Press, New York, 1969.

[8]Patankar, S. V. and Spalding, D. B., "A Calculation Procedure for Heat, Mass and Momentum Transfer in Three-Dimensional Parabolic Flows," *International Journal of Heat and Mass Transfer*, Vol. 15, 1972, pp. 1787-1806.